Available online at www.sciencedirect.com

Manufacturing Letters

Manufacturing Letters 00 (2023) 000–000

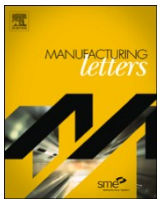

51st SME North American Manufacturing Research Conference (NAMRC 51, 2023)

A sensor-based monitoring approach to predict surface profile of vibration-assisted atomic force microscopy (AFM)-based nanofabrication

Xinchen Wang, Huimin Zhou, Jia Deng, Zimo Wang*

Department of Sytems Science and Industrial Engineering,
State University of New York at Binghamton, Binghamton, New York 13902, USA

* Corresponding author. Tel.: +1-607-777-5012. *E-mail address:* zimowang@binghamton.edu

Abstract

The vibration-assisted atomic force microscope (AFM)-based nanomachining offers a promising opportunity for low-cost nanofabrication with high tunability. However, critical challenges reside in advancing the throughput and the quality assurance of the process due to extensive offline experimental investigations and characterizations, which in turn hinders the wide industry applications of current AFM-based nanomachining process. Hence, it is necessary to create an in-process monitoring for the nanomachining to allow real-time inspection and process characterizations. This paper reports a sensor-based analytic approach to allow real-time estimations of the AFM-based nanomachining process. The temporal-spectral features of collected acoustic emission (AE) sensor signals are applied to predict the depth morphology of nanomachined trenches under different machining conditions. The experimental case study suggests that the most significant frequency domain information from AE sensor can accurately predict (R-squared value around 92%) the nanomachined depth profile. It, therefore, breaks the current limitation of characterization tools at the nanoscale precision level, and opens up an opportunity to allow real-time estimation for quality inspection of vibration-assisted AFM-based nanofabrication process.

Keywords: AFM-based nanofabrication; Nanomachining; Morphology prediction; Acoustic emissions; Sensor-based monitoring.

1. Introduction

As the demand for the shrinking size of electronic devices inside an integrated circuit chip increases, nanofabrication has been gleaning popularity in bio-production, nanolithography, and other intelligent product areas [1–4]. The atomic force microscope (AFM) has demonstrated its unique atomic-level manipulation capability to create high-quality nanostructures for nanofabrication [5,6]. The low-cost setup with exquisite tunability of AFM offers a promising opportunity for applying different methods to perform nanofabrication, such as nanomechanical nanoscratching [7,8], ultrasonic-assisted nanolithography [9], and thermochemical nanopatterning [10].

Critical challenges reside in advancing the productivity and reliability of the current AFM-based nanomachining [11]. The performance of the nanofabrication can be influenced by the setup parameters such as the properties of the treated materials and the AFM probes (e.g., spring constant of the cantilever and probe tip geometry) [12]. Providing an in-process monitoring and quality control for the nanoscale fabrication is difficult as the nanofabrication precision is within nanoscale. The fabricated nanopatterns have smaller feature sizes compared to the wavelength of light, which has limited imaging resolutions in the microscale. The nanopatterned morphology, including feature widths and depths, can only be evaluated using the AFM setup itself after the completion of the nanofabrication process [13]. This post-imaging approach cannot provide the details of the material removal timely during the nanofabrication process, which means that the performance of the fabrication and the morphology of nanopatterns, if there are any, can only be evaluated after the process [14]. No real-time morphology information can be provided while the

nanopatterning process is ongoing. In addition, the lack of temporal recordings of the process hinders the analysis of the machining parameters selections and the process characterizations: the process failures, such as AFM tip breakages and incipient anomalies (e.g., unstable vibrations/chatters), can only be noticed via post/offline characterizations [15]. The consequences of this aftermath mitigation involve costly and time-consuming rework on the workpiece. Therefore, providing real-time monitoring to evaluate the performance of the nanofabrication processes is critical to avoid unnecessary waste, improve the efficiency of quality inspection, and hence increase productivity.

Researchers have been investigating the possibility of using viable sensor setups to capture the information associated with material removals during the manufacturing processes [16]. The acoustic emission (AE) sensor captures the transient elastic wave generated by the rapid release of energy during the material removal. The characteristics of AE waveforms are highly associated with material deformation and frictions and crack propagations [17,18]. Particularly for machining processes, the different material removal mechanisms can relate to different AE signals (in amplitudes and frequency responses). In conventional machining processes, the AE temporal features [e.g., root mean squared (RMS) values] can effectively distinguish different machining conditions and materials [19] as the signals may have high resolutions [e.g., high signal-noise ratio (SNR)]. However, under the nanoscale, the AE is submerged in the noise and induced with system vibration, and conventional approaches to extract statistical features may not reflect the nanofabrication conditions accurately. Extracting prominent features of AE signal and the associated analytic tool should be introduced for the process characterizations and evaluations in the nanoscale. Enabling AE sensor monitoring scheme opens up chances for in-process inspection, machine tool wear detection, and characterizations of machining dynamics [20]. Moreover, due to its high sensitivity, the AE sensor has demonstrated its prominence in monitoring material removals at the nanoscale [21–23]. However, the AE signal gathered during AFM-based nanomachining has not been fully explored toward in-process morphology characterizations and predictions.

In this paper, we present an analytic approach that allows in-process prediction of surface profiles, specifically the cutting depths, via the AE sensor-based monitoring scheme. The approach was tested based on the experimental case study of the vibration-assisted AFM-based nanomachining of polymethyl methacrylate (PMMA) samples. The remainder of the paper is organized as follows: Sec. 2 presents the hardware setup and data collection process from the sensor. The analytic approach to capture the surface morphology of the nanofabrication via sensor-based monitoring acoustic emission signals is introduced in Sec. 3. The results of the experimental case study and the discussions are in Sec. 4, followed by the concluding remarks in Sec. 5.

2. Experimental setup and data collection

2.1. Hardware setup and the experiments

This vibration-assisted AFM-based nanomachining experiment was performed on a customized nanovibrator stage within a commercial AFM system (XE7, Park Systems Corporation, Suwon, South Korea), as shown in Figure 1. To generate the in-plane vibrations for the nanomachining process, two piezoelectric actuators are installed on the bottom of the aluminum pillar which is used to place the sample. PMMA sample with 200 nm thickness was spin-coated on silicon substrates with post-bake at 180˚C for 90 seconds. DLC190 AFM probe was used to fabricate and image the nanotrenches on the PMMA sample. A signal generator (USB-6259, National Instruments, Austin, TX, USA) and two signal amplifiers (PX200, PiezoDrive, Shortland, NSW, Australia) are used to generate input signals for the piezoelectric actuators, which create in-plane circular xy-vibration (with intrinsic frequency of 2 kHz) on the sample based on two sinusoid waveforms with 90-degree phase shift. An AE sensor (s9225 from Physical Acoustics, Princeton Jct, NJ, USA) is installed under the sample mounting plate, and a data acquisition (DAQ) system (using the NI-USB-6259) is applied to collect the AE signal with 500k Hz sample rate during the nanomachining process.

To validate the contribution of sensor-based tech for nanoscale process monitoring, a set of nanomachining experiments is devised with varying cutting forces (50, 150, 250, 350, and 450 nNs) on a PMMA sample surface with a machining length of about 1 μm. The surface morphology of the nanotrenches fabricated with different normal forces is shown in Figure 2. To illustrate the significant features (width and depth) in Figure 2 a), the cross-sectional profile of the five nanotrenches at the 0.8 μm y-axis, marked with a red line, is shown in Figure 2 b). The temporal AE signals of five cuts are collected by the mounted AE sensor, which is used to investigate the validity of the sensor-based method in the monitoring process with different nanofabrication conditions.

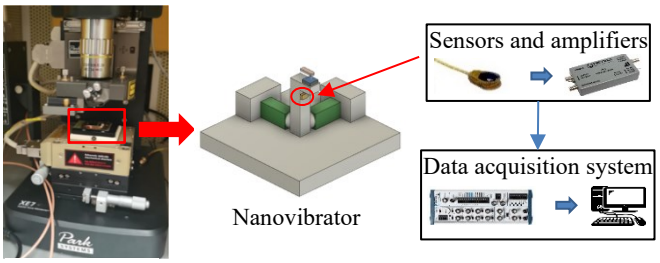

Figure 1. The AE sensor and data acquisition system integrated with the vibration-assisted AFM-based nanofabrication platform.

2.2. Data description

This investigation tries to present an analytic model that connects the acoustic emission phenomena and the fundamental mechanisms of material removals during the nanofabrication. To test the capability of the monitoring setup for characterizations of nanofabrication, the spectral features of gathered AE signals during the nanomachining are used to associate the temporal modifications during the nanomachining process; the surface characteristics, in terms of cutting depths, of nanofabricated trenches, are selected as the responses.

The cutting depth coordinates are regarded as the dependent variable for the prediction model which can be used to describe one of the typical features of the cuts' morphology. Meanwhile,

acoustic emission (AE) signals, are synchronously captured by the sensor during the cutting operation, which can be treated as the independent variables for the prediction model.

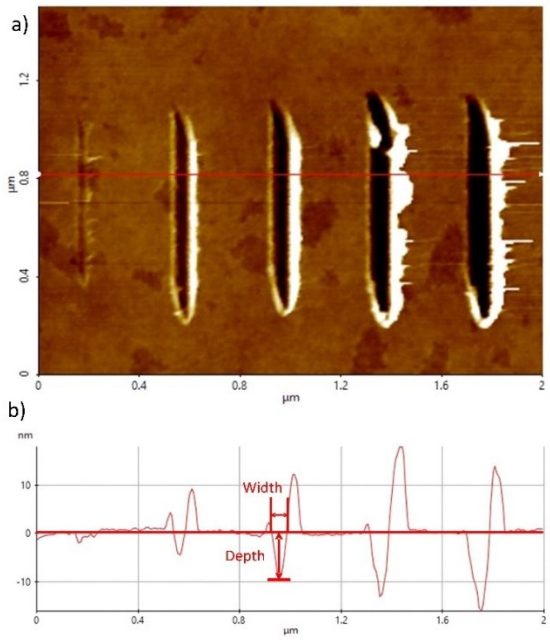

Figure 2. a) Five nanomachined trenches. b) Cross-sectional profile with widths and depths of the trenches.

The surface morphology of five trenches is extracted from the machined samples scanned by the AFM. The total sample area is 2×1.5 micrometers, and 1200 sample data points are collected on each direction axis. The length of each segmentation unit on each axis ranges from 1.25nm to 1.70 nm, as shown in Figure. 3. The five cuts from left to right are machined by various forces (50, 150, 250, 350, and 450 nNs), and the heavier force causes a deeper cut, which can be reflected from the color in Figure. 3. The dark color represents the deeper part and the light color represents the higher parts. the width and depth of cuts are marked in Figure. 3. a) and c), the cutting direction is marked on Figure. 3. b) and d). The extracted surface profile and the cutting depth (surface profile along the vertical direction) are shown in Figure. 4.

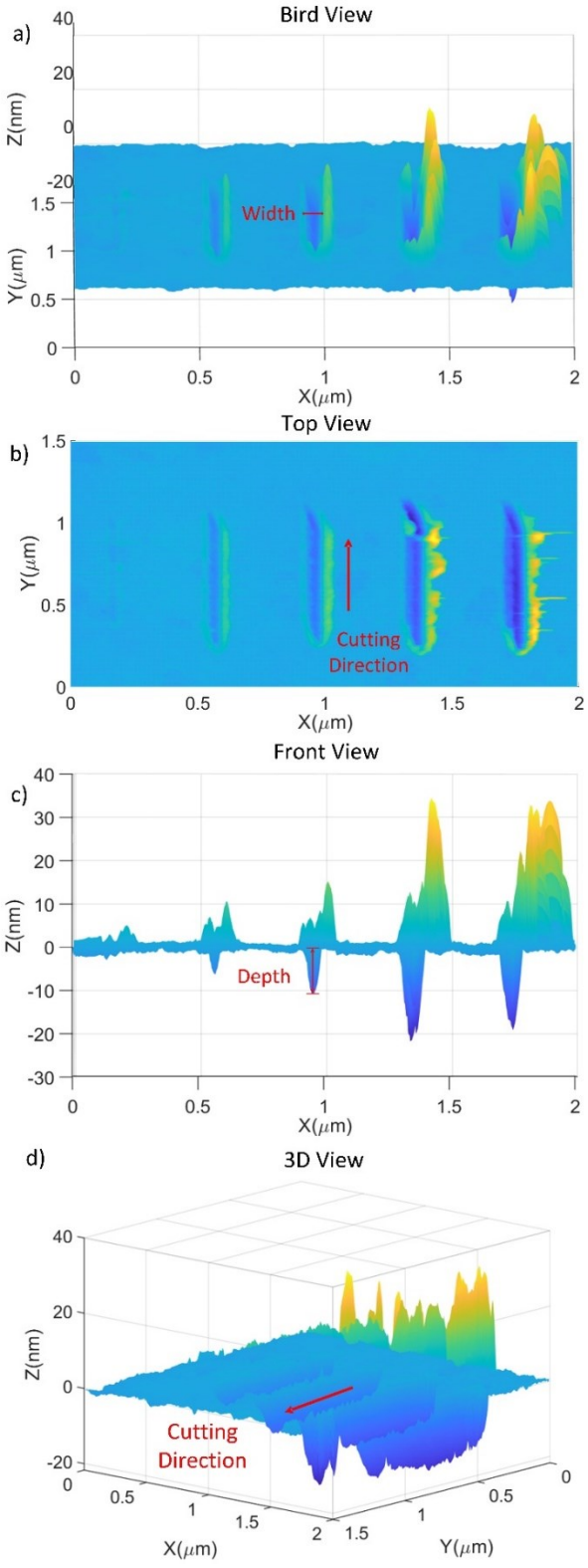

Figure 3. a) Bird view of 3D surface profiles of trenches. b) Top view of 3D surface profiles of trenches. c) Front view of 3D surface profiles of trenches. d) 3D surface profiles of trenches.

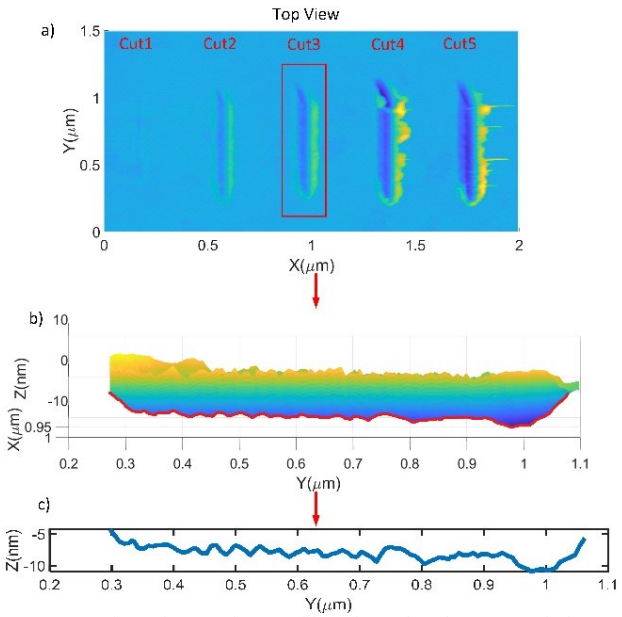

Figure 4. a) Top view of 3D surface profiles of trenches. b) 3D morphology of Cut 3. c) Depth line of Cut 3.

Figure. 4. shows, in total, five cuts (Cuts 1 to 5 from left to right). To show the machined surface morphology, Cut 3 is selected as an example. Figure 4 b) shows the 3D morphology of Cut 3. The instantaneous depth of cut is depicted in the red line in Figure 4 b). Predicting the depth of cut based on the sensor signals is critical for in-process evaluations of the nanofabrication quality. The 3D cut figure is projected to the y-axis and z-axis coordinates, and the depth line is shown in the coordinate area in Figure 4 c).

The synchronized AE sensor signals during the nanomachining are shown in Figure. 5. The AE signal always exhibits highly nonstationary and transient behaviors that capture the acoustic emission phenomena during the material removals. The most significant spectral AE features in distinguishing differences between cutting conditions are highly correlated to the failure modes of PMMA materials. To analyze the AE signal, its temporal-spectral features are extracted to evaluate the frequency responses during the nanomachine. It applies a sliding window for Fast Fourier transformation (FFT) to extract the time-frequency features from AE signals. The represented temporal-spectral features are shown in Figure 5, of which the x-axis is the time index and the y-axis is the frequency range, and the energy of various frequency bands (in dB) is represented using a color map. To analyze the AE spectral responses in high resolution, 4095 different frequency bands of AE signal are generated within the range from 0 to 250 kHz (see Figure 5). It is impractical that all the 4095 frequency bands are involved in the machine learning model, and due to the noise and system vibrations, only critical frequency bands are sensitive to the cutting process which can be used for the prediction. Therefore, feature selection is an unavoidable step in this problem.

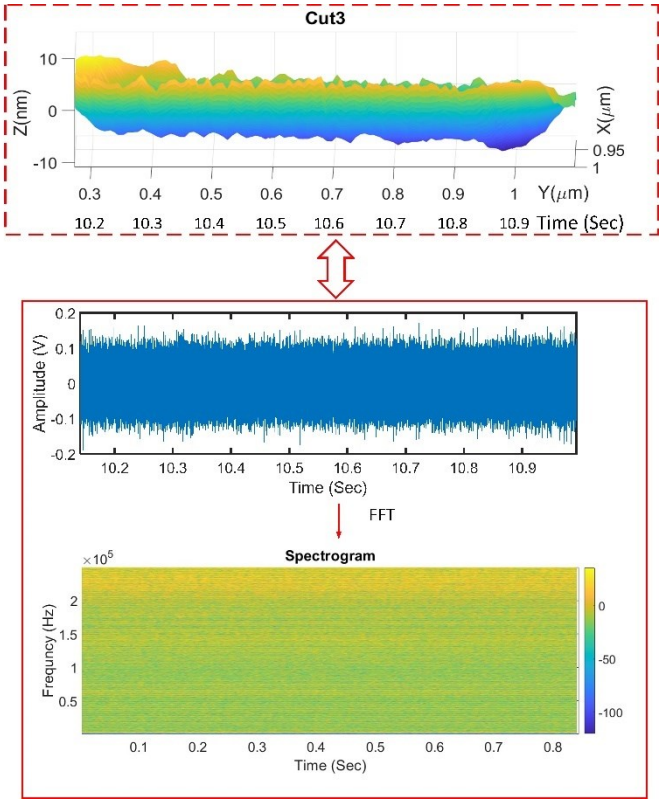

Figure 5. The nanomachine trench (shown with the depth profile) with synchronously gathered AE signal during the nanomachining. The spectrogram shows the frequency component variations during the nanomachining process.

To help select useful spectral features, a random forest classification approach is applied. This classification algorithm implicitly selects the features (subsets of frequency bands) that contribute most to the classification of different cutting conditions. Intuitively speaking, the most distinguishable frequency domain information associates with different energy responses of AE signals during the nanomachining [23].

Top twenty significant features selected from the random forest classification model are regarded as the independent variables for the inputs in the prediction model, and the depths of cut are taken as the dependent variable. These data are applied to the multivariate linear regression model, and the fitted model can apply to make the prediction for the depths of different trenches.

3. Methodology

For the feature selection, fast Fourier transformation (FFT) is used to convert five cuts' AE signals to the temporal-spectral domain.

In FFT process, the sliding windows with the window length N=5000 (with time duration of 10 milliseconds) are introduced to capture a set of AE signal at time index t, i.e., $\{x_{t-N+1}, x_{t-N+2}, \dots, x_t\}$.

The temporal-frequency relationship in FFT can be formulated as:

$$X_k^{(t)} = \sum_{n=t-N+1}^{t} x_n e^{-\frac{i2\pi kn}{N}} \quad k = 0, \dots, N-1 \tag{1}$$

x_n is the temporal AE signal which can be represented as $\{x_n, n = t-N+1, t-N+2, \dots t\}$ in a sliding window, the FFT converts the signal to the frequency components

$\boldsymbol{X}^{(t)} = [X_1^{(t)}, X_2^{(t)}, \dots, X_N^{(t)}]^T$. With the movement of the sliding window, the set of all windows' frequency components can be represented as $\boldsymbol{R} = [\boldsymbol{X}^{(N)}, \boldsymbol{X}^{(N+S)}, \dots, \boldsymbol{X}^{M}]$, S is the step of the sliding window and M denotes the discrete time index after transformation. $\boldsymbol{R}$ records the magnitudes of the Fourier which can represent the matrix of the signal spectrogram.

In the spectrogram figure, the x-axis represents the time and y-axis represents the different frequency bands. The energy of the frequency bands at various time is depicted by the color map. The frequency range for the signal is depended on the sample rate of the FFT which is 500 kHz, the signal frequency range is also half of the sample rate. Essentially, the energy of the spectrum in various frequency bands is related to the nanomachining process which, can be written as $\boldsymbol{F}^{(i)} = E_1^{(i)}, E_2^{(i)}, \dots, E_w^{(i)}]$, $i = 1,2 \dots, b, w = 1,2, \dots, M$, where $\boldsymbol{F}^{(i)}$ represents the frequency band, E_w represents the energy at various times, b represents the frequency bands' index for the signal. The $\boldsymbol{R}$ matrix also can be represented by frequency bands which can be written as $\boldsymbol{R} = [\boldsymbol{F}^{(1)}, \boldsymbol{F}^{(2)}, \dots, \boldsymbol{F}^{(b)}]$, and each frequency band can represent a signal feature in the classification model. The $\boldsymbol{R}$ matrix can be illustrated with symbols in Figure. 6.

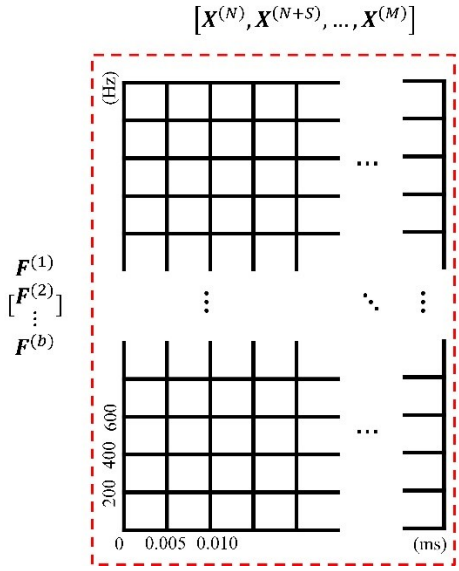

Figure 6. The notations for the extracted temporal spectral features.

In order to find the most significant features, a random forest classification approach is used to distinguish the different cuts and non-cuts' depth and order the most important spectral information contributing to the classification problem. For the five cuts with different depths, the mean value of each cut depth is used to represent the cutting classification label and replaces the cutting depths' coordinates values, the non-cut' depth is donated to zero. Depth coordinates of cut can be written as $C = \{c_1, c_2, \dots c_z\}$, where z represents the coordinates for the cut's depth, the dependent variable depth is written as $\boldsymbol{Y} = [C_I, C_{II}, C_{III}, C_{IV}, C_V, C_{non}]^T$ ($\{I, II, III, IV, V, non\}$ is the index of the five different cut and non-cut), which assembles five cuts and non-cut's depth coordinate values.

In the classification model, the cuts and non-cuts' depths coordinates are regarded as the responses for the classification labels, and the corresponding spectral features of cuts and non-cut's AE signal are taken as the predictors which can be written as $\boldsymbol{X} = [\boldsymbol{R}^{(I)}, \boldsymbol{R}^{(II)}, \boldsymbol{R}^{(III)}, \boldsymbol{R}^{(IV)}, \boldsymbol{R}^{(V)}, \boldsymbol{R}^{(non)}]$.

During the training process, the random forest approach generates several decision tree models to train the bootstrapped data samples. Each data sample set is selected randomly from the original data with replacement, and the number of samples in each set is same as the original set $\{\boldsymbol{X}\}$ and $\{\boldsymbol{Y}\}$. The features are randomly sampled and the best split among these selected predictors is chosen for each node of the tree models. Assuming that the splitting variable X_j is split at point x_j to segment the predictor set. The voting mechanism of random forest can finally classify each independents variables set to the corresponding classifications. Meanwhile, random forest method performs a feature selection by using the subset of the $\{X_j\}$ in classification problem. The Gini important values for each feature $\boldsymbol{F^{(b)}}$ in matrix $\boldsymbol{R}$ will be calculated and ranked to show the relevance to the classification results [24].

The Gini impurity $Gini(\eta)$ equation can be formulated as:

$$Gini(\eta) = 1 - \sum_c p_c^2 \tag{2}$$

$P_c = n_c/n$ represents the fraction of the n_c samples from the class $Cut = \{Cut1, Cut2, Cut3, Cut4, Cut5, Cut\_non\}$ ($c \in Cut1, Cut2, Cut3, Cut4, Cut5, Cut_{non}$) of the total n sample at node η.

The decrease $\Delta\, Gini$ which results from splitting and sending the samples to sub-nodes η_l and η_r (with respective sample fractions $p_l = n_l/n$ and $p_r = n_r/n$). The function can be written as:

$$\Delta Gini(\eta) = Gini(\eta) - p_l Gini(\eta_l) - p_r Gini(\eta_r) \tag{3}$$

In an exhaustive search over all variables X_j at the nodes and over all possible thresholds x_j obtains a pair $\{X_j, x_j\}$, which leads to a maximal $\Delta Gini$ value. The decrease in Gini impurity is accumulated for all nodes η in all trees D in the forest, individually for all variables F_j:

$$I_{Gini}(X_j) = \sum_D \sum_\eta \Delta Gini_{\{X_j\}}(\eta, D) \tag{4}$$

The I_{Gini} can suggest how often a feature is selected for a split, which can be regarded as criteria to evaluate the importance of the features.

The classification results of the random forest model are shown in Figure. 7, and important values' scores for the features are shown in Figure. 8.

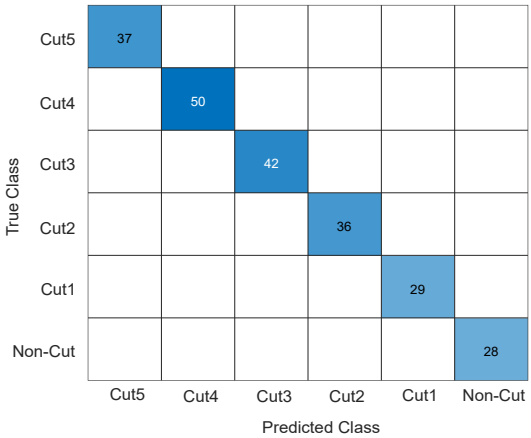

Figure 7. The classifications using the temporal spectral features on characterizations of different cutting conditions.

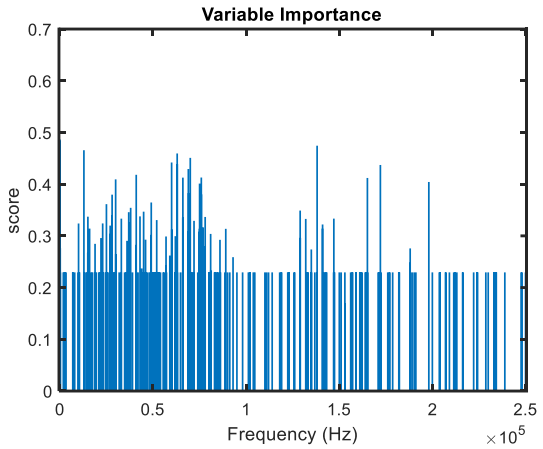

Figure 8. Scores of frequency domain information on distinguishing different nanomachining condition.

In Figure. 7, the classification result shows that random forest method can perfectly classify the cut's depth with the temporal-spectral feature of AE signal, and Figure. 8. can illustrate that the frequency bands around 50kHz and 150kHz have significant contributions to the classification problem. Based on the classification results and features' score, several temporal-frequency features have significant contributions to the cuts' depth recognition.

To reduce the calculation time and cost, the features' scores are ranked from top to bottom and only some top features are selected for the classification model. After multiple model fitting tests, top twenty features (frequency bands) can successfully classify the depths of the cut, which means that the top twenty frequency bands have enough information for the cutting depths' prediction.

Therefore, the cut depth prediction model will only pick the top twenty important frequency band features $\{\boldsymbol{F}^{t1}, \boldsymbol{F}^{t2}, \dots, \boldsymbol{F}^{t20}\}$ as the independent variables. The top twenty frequencies for each cut will be extracted from their spectrogram matrix separately, and the twenty frequency bands will be regarded as twenty predictors in the multivariate linear regression. The predictors (using the top twenty most significant spectral features) can be represented as $\boldsymbol{P}_h = [\boldsymbol{F}_I^{th}, \boldsymbol{F}_{II}^{th}, \dots, \boldsymbol{F}_V^{th}]^T, h = 1,2,3\dots,20$.

Multivariate linear regression can solve the prediction problem with multiple independent variables. The prediction formulation can be expressed as:

$$Y = \alpha + \beta_1 x_1 + \beta_2 x_2 + \cdots + \beta_n x_n \quad (5)$$

Y is the response value, the x_1 to x_n are the n distinct independent variables, the β_1 to β_2 are the regression coefficients, the α is the value of Y when all the predictors equal zero. To fit the prediction model, the top twenty frequency bands of each cut are treated as twenty predictor variables, and the depth coordinates for each cut are matched to the response of the model. The model can be represented as:

$$[C_I, C_{II}, \dots, C_V,]^T = \alpha + \beta_1 \boldsymbol{P}_1 + \beta_2 \boldsymbol{P}_2 + \cdots + \beta_{20} \boldsymbol{P}_{20} \quad (6)$$

After model training, the cut's temporal-frequency feature of the AE signal will be used to predict the cut's depth. All frequency features of the five cuts will be separated into 80% training data and 20% testing data, and the R squared and RMSE (root-mean-square deviation) methods will be used to evaluate the stability of the model. In addition, the original depth's coordinates and predicted depth's coordinates will also be compared and discussed in the next part.

4. Results and Discussions

To validate the prediction method for estimating surface profile in nanoscale, the five cuts' depths are extracted from the trenches' surface profiles, and the corresponding top twenty important frequency features for each cut are selected as the predictors for the multivariate linear regression. The original depth and predicted depth of the training model and testing model are shown in Figure. 9, the black line (Y_{train}) represents the original depth line and the red line represents the predicted line (P_{train}), The green line (Y_{test}) is the original depth line and the blue one (P_{test}) is the predicted results for the testing data.

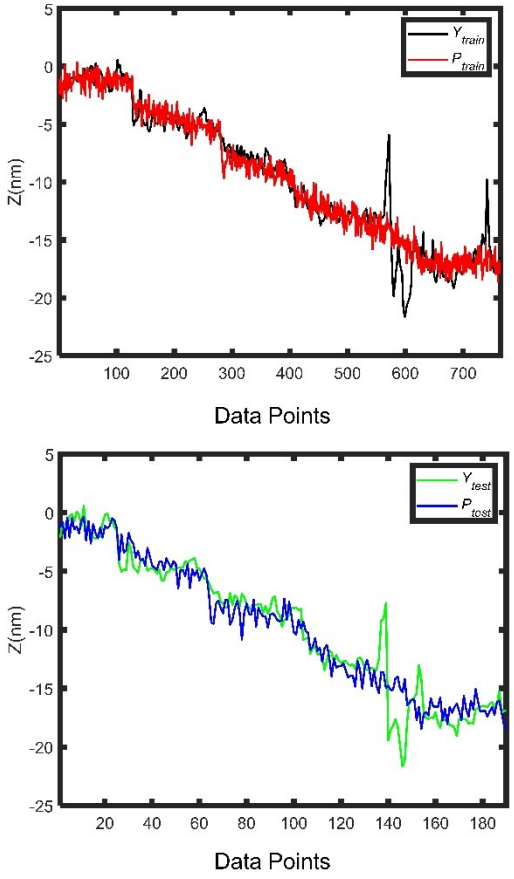

Figure 9. The prediction results using the presented analytic approach with a) training and b) testing datasets: a) The ground truth is plotted in black and the predicted values are portraited in red lines; b) The ground truth of the testing set is depicted in green and the predicted values are shown in blue lines.

The prediction results are shown in Figure. 9. and Table 1. To validate the effectiveness of the model, the R squared and RMSE are introduced to evaluate the performance of the model. R squared is a statistical measure of fit that indicates how much variation of a dependent variable is explained by the independent variables in a regression model. Therefore, the R squared can suggest whether the temporal-frequency of AE signal can reflect the depth feature of the cuts. RMSE is a used measure of the differences between values predicted by a model and the values observed, which values can prove the accuracy of the model.

To test the stability of the model, the training and testing data are randomly selected ten times without the proportion change in the dataset, and the model is fitted ten times with different training and testing data. The quartiles, variance and

mean values of the ten models' R squared and RMSE are shown in Table 1.

As for the training phase, the prediction model obtained a high R-squared value (see Table 1), which indicates that the independent variable (frequency features of the AE signal) can explain almost 92% variation of the cutting depths; the prediction results as shown in Figure 9 b), where the blue line is the predicted value and the green line is the ground truth of the surface profile, suggest that the presented approach can accurately predict the tendency of the surface profile, in terms of the cutting depths. In addition, the RMSE achieves a mean of 0.0161 based on ten computations, which verifies that the approach is stable for inferencing the machined profiles based on AE signals.

Table 1. Statistic description for R squared and RMSE for predicted model.

	Q1	Q2	Q3	Q4	Variance	Mean
R Squared	0.8974	0.9127	0.9371	0.9373	0.0002	0.9237
RMSE	0.0144	0.0150	0.0175	0.0184	0.0000	0.0161

Next, we show the capability of the presented approach on creating a real-time cyber-twin of the surface profile. In Figure. 10, the real cuts' depths line (Y) and their predicted depths line (Y_{hat}) are compared. The black dot line is the predicted results and the red line is the original depths line.

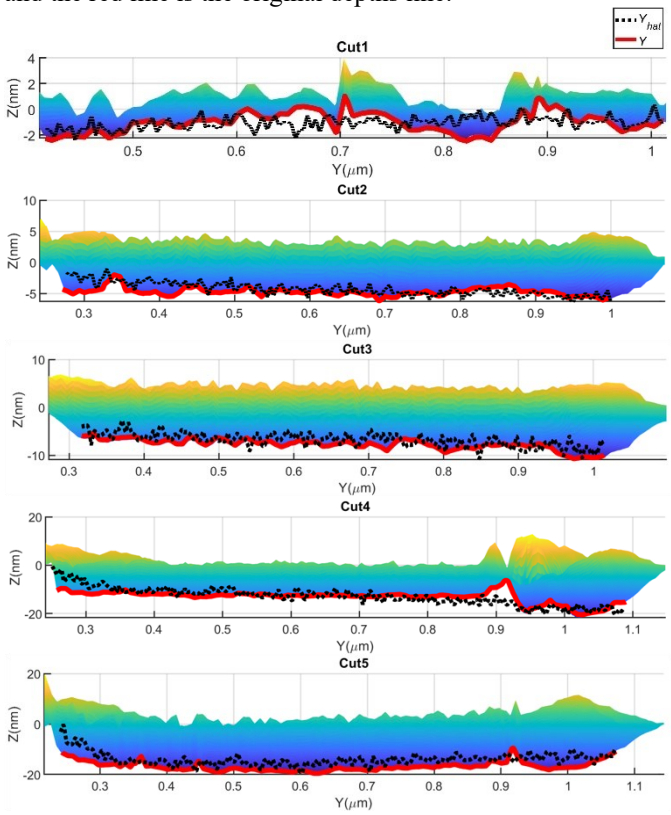

Figure 10. The results comparisons between the ground truth (surface profile in the color map and the surface depth in the red line) and predicted depth profile plotted in black dash line.

Based on the cutting depths figure, the predicted depths of the training model and testing model can mostly depict the variety and the tendency of the original cutting depths without certain dramatic changes and machining errors. The R-squared value and RMSE value suggest that the multivariate linear regression can output stable predicted results with high accuracy. Therefore, it is evidenced that the temporal-spectral feature of the nanomachine process can be used to characterize and predict the nanomachine surface morphology.

5. Conclusion

This paper presents an AE sensor-based monitoring approach for in-process estimation of the surface profiles by vibration-assisted AFM-based nanomachining. The main contribution of this paper can be summarized as follows:

1. The AE sensor-based monitoring approach for the nanofabrication process is discussed in this paper. Further investigations suggest that the temporal-spectral features of AE signals are highly related to recognize different machining conditions in terms of cutting depths during the AFM-based nanofabrication.

2. The random forest algorithm was applied to classify the cut and non-cut nanofabrication conditions. Based on the importance values generated by the random forest model, the most significant AE spectral features that contribute to distinguish different cutting conditions are selected as the predictors for estimating the in-process surface morphology using a multivariate linear regression model.

3. The experimental case study suggests that the selected spectral features can predict the surface profile in terms of the cutting depth, and the variations under different cutting forces (within the range of nano-Newtons). The prediction model achieves an R-squared value of more than 92% to accurately estimate the surface profile at the nanoscale achieved by the AFM-based nanofabrication.

In brief, the presented AE sensor-based monitoring approach breaks the current limitation of characterization tools at the nanoscale precision level. It hence opens up an opportunity to allow real-time estimation of the machining quality of AFM-based nanofabrication process.

In future, advanced approaches toward selection AE characteristics will be incorporated to advance the prediction accuracy for building the digital-twin of AFM-based nanofabrication. The physical informed analytic model will be further investigated to predict other surface profile quantifiers such as the cutting width and the overall morphology with complicated 2D/3D patterns.

Acknowledgement

This work was partly supported by the National Science Foundation under grant No. CMMI-2006127, and by the Small Scale Systems Integration and Packaging (S3IP) Center of Excellence, funded by the New York Empire State Development's Division of Science, Technology, and Innovation.

6. Reference

[1] Garg A, Mejia E, Nam W, Nie M, Wang W, Vikesland P, et al. Microporous Multiresonant Plasmonic Meshes by Hierarchical Micro–Nanoimprinting for Bio-Interfaced SERS Imaging and Nonlinear Nano-Optics. Small 2022;18:2106887.

[2] Mathew PT, Rodriguez BJ, Fang F. Atomic and Close-to-Atomic Scale Manufacturing: A Review on Atomic

Layer Removal Methods Using Atomic Force Microscopy. Nanomanufacturing Metrol 2020;3:167–86.

[3] Ortlepp I, Stauffenberg J, Krötschl A, Dontsov D, Zöllner J-P, Hesse S, et al. Nanofabrication and -metrology by using the nanofabrication machine (NFM-100). In: Panning EM, Liddle JA, editors. Nov. Patterning Technol. 2022, San Jose, United States: SPIE; 2022, p. 30.

[4] Yao B, Chen C, Du Z, Qian Q, Pan L. Surfing Scanning Probe Nanolithography at Meters Per Second. Nano Lett 2022;22:2187–93.

[5] Rangelow IW, Kaestner M, Ivanov T, Ahmad A, Lenk S, Lenk C, et al. Atomic force microscope integrated with a scanning electron microscope for correlative nanofabrication and microscopy. J Vac Sci Technol B 2018;36:06J102.

[6] Geng Y, Yan Y, He Y, Hu Z. Investigation on friction behavior and processing depth prediction of polymer in nanoscale using AFM probe-based nanoscratching method. Tribol Int 2017;114:33–41.

[7] Tian Y, Lu K, Wang F, Guo Z, Zhou C, Liang C, et al. Design of a novel 3D tip-based nanofabrication system with high precision depth control capability. Int J Mech Sci 2020;169:105328.

[8] Stauffenberg J, Ortlepp I, Reuter C, Holz M, Dontsov D, Schäffel C, et al. Investigations on Long-Range AFM Scans Using a Nanofabrication Machine (NFM-100). 4th Int. Conf. NanoFIS 2020 - Funct. Integr. Nanosyst., MDPI; 2020, p. 34.

[9] Deng J, Dong J, Cohen PH. Development and Characterization of Ultrasonic Vibration Assisted Nanomachining Process for Three-Dimensional Nanofabrication. IEEE Trans Nanotechnol 2018;17:559–66.

[10] Zheng X, Calò A, Albisetti E, Liu X, Alharbi ASM, Arefe G, et al. Patterning metal contacts on monolayer MoS2 with vanishing Schottky barriers using thermal nanolithography. Nat Electron 2019;2:17–25.

[11] Tseng AA. Advancements and challenges in development of atomic force microscopy for nanofabrication. Nano Today 2011;6:493–509.

[12] Ren J, Yue H, Liang G, Lv M. Influence of Tool Shape on Surface Quality of Monocrystalline Nickel Nanofabrication. Molecules 2022;27:603.

[13] Zhou H, Jiang Y, Dmuchowski CM, Ke C, Deng J. Electric-Field-Assisted Contact Mode Atomic Force Microscope-Based Nanolithography With Low Stiffness Conductive Probes. J Micro Nano-Manuf 2022;10.

[14] Verna E, Genta G, Galetto M, Franceschini F. Planning offline inspection strategies in low-volume manufacturing processes. Qual Eng 2020;32:705–20.

[15] Zavedeev EV, Jaeggi B, Zuercher J, Neuenschwander B, Zilova OS, Shupegin ML, et al. Effects of AFM tip wear on frictional images of laser-patterned diamond-like nanocomposite films. Wear 2018;416–417:1–5.

[16] Rao PK, Liu J (Peter), Roberson D, Kong Z (James), Williams C. Online Real-Time Quality Monitoring in Additive Manufacturing Processes Using Heterogeneous Sensors. J Manuf Sci Eng 2015;137.

[17] Du K, Li X, Tao M, Wang S. Experimental study on acoustic emission (AE) characteristics and crack classification during rock fracture in several basic lab tests. Int J Rock Mech Min Sci 2020;133:104411.

[18] Lockner D. The role of acoustic emission in the study of rock fracture. Int J Rock Mech Min Sci Geomech Abstr 1993;30:883–99.

[19] Lee DE, Hwang I, Valente CMO, Oliveira JFG, Dornfeld DA. Precision manufacturing process monitoring with acoustic emission. Int J Mach Tools Manuf 2006;46:176–88. https://doi.org/10.1016/j.ijmachtools.2005.04.001.

[20] Kishawy HA, Hegab H, Umer U, Mohany A. Application of acoustic emissions in machining processes: analysis and critical review. Int J Adv Manuf Technol 2018;98:1391–407.

[21] Lee DE, Hwang I, Valente CMO, Oliveira JFG, Dornfeld DA. Precision Manufacturing Process Monitoring with Acoustic Emission. In: Wang L, Gao RX, editors. Cond. Monit. Control Intell. Manuf., London: Springer; 2006, p. 33–54.

[22] Lee SH. Analysis of ductile mode and brittle transition of AFM nanomachining of silicon. Int J Mach Tools Manuf 2012;61:71–9.

[23] Ma Q, Zhou H, Deng J, Wang Z. Characterizing vibration-assisted atomic force microscopy (AFM)-based nanomachining via perception of acoustic emission phenomena using a sensor-based real-time monitoring approach. Manuf Lett 2022;34:6–11.

[24] Wang Z, Chegdani F, Yalamarti N, Takabi B, Tai B, El Mansori M, et al. Acoustic Emission Characterization of Natural Fiber Reinforced Plastic Composite Machining Using a Random Forest Machine Learning Model. J Manuf Sci Eng 2020;142:031003.